



## **AMADEUS - The Acoustic Neutrino Detection Test System of the Deep-Sea ANTARES Neutrino Telescope**

J.A. Aguilar, I. Al Samarai, A. Albert, M. Anghinolfi, G. Anton, S. Anvar, M. Ardid, A.C. Assis Jesus, T. Astraatmadja, J.-J. Aubert, et al.

### **► To cite this version:**

J.A. Aguilar, I. Al Samarai, A. Albert, M. Anghinolfi, G. Anton, et al.. AMADEUS - The Acoustic Neutrino Detection Test System of the Deep-Sea ANTARES Neutrino Telescope. Nuclear Instruments and Methods in Physics Research Section A: Accelerators, Spectrometers, Detectors and Associated Equipment, Elsevier, 2010, 626-627, pp.128-143. <10.1016/j.nima.2010.09.053>. <in2p3-00474914>

**HAL Id: in2p3-00474914**

**<http://hal.in2p3.fr/in2p3-00474914>**

Submitted on 21 Apr 2010

**HAL** is a multi-disciplinary open access archive for the deposit and dissemination of scientific research documents, whether they are published or not. The documents may come from teaching and research institutions in France or abroad, or from public or private research centers.

L'archive ouverte pluridisciplinaire **HAL**, est destinée au dépôt et à la diffusion de documents scientifiques de niveau recherche, publiés ou non, émanant des établissements d'enseignement et de recherche français ou étrangers, des laboratoires publics ou privés.



# AMADEUS - The Acoustic Neutrino Detection Test System of the Deep-Sea ANTARES Neutrino Telescope

J.A. Aguilar<sup>a</sup>, I. Al Samarai<sup>b</sup>, A. Albert<sup>c</sup>, M. Anghinolfi<sup>d</sup>,  
G. Anton<sup>e</sup>, S. Anvar<sup>f</sup>, M. Ardid<sup>g</sup>, A.C. Assis Jesus<sup>h</sup>,  
T. Astraatmadja<sup>h,1</sup>, J-J. Aubert<sup>b</sup>, R. Auer<sup>e</sup>, E. Barbarito<sup>i</sup>, B. Baret<sup>j</sup>,  
S. Basa<sup>k</sup>, M. Bazzotti<sup>l,m</sup>, V. Bertin<sup>b</sup>, S. Biagi<sup>l,m</sup>, C. Bigongiari<sup>a</sup>,  
M. Bou-Cabo<sup>g</sup>, M.C. Bouwhuis<sup>h</sup>, A. Brown<sup>b</sup>, J. Brunner<sup>b,2</sup>,  
J. Busto<sup>b</sup>, F. Camarena<sup>g</sup>, A. Capone<sup>n,o</sup>, C.Cârloganu<sup>p</sup>,  
G. Carminati<sup>l,m</sup>, J. Carr<sup>b</sup>, B. Cassano<sup>i</sup>, E. Castorina<sup>q,r</sup>,  
V. Cavasinni<sup>q,r</sup>, S. Cecchini<sup>m,s</sup>, A. Ceres<sup>i</sup>, Ph. Charvis<sup>t</sup>,  
T. Chiarusi<sup>m</sup>, N. Chon Sen<sup>c</sup>, M. Circella<sup>i</sup>, R. Coniglione<sup>u</sup>,  
H. Costantini<sup>d</sup>, N. Cottini<sup>v</sup>, P. Coyle<sup>b</sup>, C. Curtil<sup>b</sup>, G. De Bonis<sup>n,o</sup>,  
M.P. Decowski<sup>h</sup>, I. Dekeyser<sup>w</sup>, A. Deschamps<sup>t</sup>, C. Distefano<sup>u</sup>,  
C. Donzaud<sup>j,x</sup>, D. Dornic<sup>b,a</sup>, D. Drouhin<sup>c</sup>, T. Eberl<sup>e</sup>,  
U. Emanuele<sup>a</sup>, J-P. Ernenwein<sup>b</sup>, S. Escoffier<sup>b</sup>, F. Fehr<sup>e</sup>,  
V. Flaminio<sup>q,r</sup>, U. Fritsch<sup>e</sup>, J-L. Fuda<sup>w</sup>, P. Gay<sup>p</sup>, G. Giacomelli<sup>l,m</sup>,  
J.P. Gómez-González<sup>a</sup>, K. Graf<sup>e</sup>, G. Guillard<sup>y</sup>, G. Halladjian<sup>b</sup>,  
G. Hallewell<sup>b</sup>, H. van Haren<sup>z</sup>, A.J. Heijboer<sup>h</sup>, E. Heine<sup>h</sup>,  
Y. Hello<sup>t</sup>, J.J. Hernández-Rey<sup>a</sup>, B. Herold<sup>e</sup>, J. Hößl<sup>e</sup>,  
M. de Jong<sup>h,1</sup>, N. Kalantar-Nayestanaki<sup>aa</sup>, O. Kalekin<sup>e</sup>,  
A. Kappes<sup>e</sup>, U. Katz<sup>e</sup>, P. Keller<sup>b</sup>, P. Kooijman<sup>h,ab,ac</sup>, C. Kopper<sup>e</sup>,  
A. Kouchner<sup>j</sup>, W. Kretschmer<sup>e</sup>, R. Lahmann<sup>e,\*</sup>, P. Lamare<sup>f</sup>,  
G. Lambard<sup>b</sup>, G. Larosa<sup>g</sup>, H. Laschinsky<sup>e</sup>, H. Le Provost<sup>f</sup>,  
D. Lefèvre<sup>w</sup>, G. Lelaizant<sup>b</sup>, G. Lim<sup>h,ac</sup>, D. Lo Presti<sup>ad</sup>,  
H. Loehner<sup>aa</sup>, S. Loucatos<sup>v</sup>, F. Louis<sup>f</sup>, F. Lucarelli<sup>n,o</sup>,  
S. Mangano<sup>a</sup>, M. Marcelin<sup>k</sup>, A. Margiotta<sup>l,m</sup>,  
J.A. Martinez-Mora<sup>g</sup>, A. Mazure<sup>k</sup>, M. Mongelli<sup>i</sup>, T. Montaruli<sup>i,ae</sup>,  
M. Morganti<sup>q,r</sup>, L. Moscoso<sup>v,j</sup>, H. Motz<sup>e</sup>, C. Naumann<sup>v</sup>, M. Neff<sup>e</sup>,  
R. Ostasch<sup>e</sup>, D. Palioselitis<sup>h</sup>, G.E.Păvălaș<sup>af</sup>, P. Payre<sup>b</sup>,  
J. Petrovic<sup>h</sup>, N. Picot-Clemente<sup>b</sup>, C. Picq<sup>v</sup>, V. Popa<sup>af</sup>, T. Pradier<sup>y</sup>,  
E. Presani<sup>h</sup>, C. Racca<sup>c</sup>, A. Radu<sup>af</sup>, C. Reed<sup>b,h</sup>, G. Riccobene<sup>u</sup>,

C. Richardt<sup>e</sup>, M. Rujoiu<sup>af</sup>, M. Ruppi<sup>i</sup>, G.V. Russo<sup>ad</sup>, F. Salesa<sup>a</sup>,  
P. Sapienza<sup>u</sup>, F. Schoeck<sup>e</sup>, J-P. Schuller<sup>v</sup>, R. Shanidze<sup>e</sup>,  
F. Simeone<sup>o</sup>, M. Spurio<sup>ℓ,m</sup>, J.J.M. Steijger<sup>h</sup>, Th. Stolarczyk<sup>v</sup>,  
M. Taiuti<sup>ag,d</sup>, C. Tamburini<sup>w</sup>, L. Tasca<sup>k</sup>, S. Toscano<sup>a</sup>, B. Vallage<sup>v</sup>,  
V. Van Elewyck<sup>j</sup>, G. Vannoni<sup>v</sup>, M. Vecchi<sup>n</sup>, P. Vernin<sup>v</sup>,  
G. Wijnker<sup>h</sup>, E. de Wolf<sup>h,ac</sup>, H. Yepes<sup>a</sup>, D. Zaborov<sup>ah</sup>,  
J.D. Zornoza<sup>a</sup>, J. Zúñiga<sup>a</sup>

- <sup>a</sup>IFIC - Instituto de Física Corpuscular, Edificios Investigación de Paterna, CSIC - Universitat de València, Apdo. de Correos 22085, 46071 Valencia, Spain
- <sup>b</sup>CPPM - Centre de Physique des Particules de Marseille, CNRS/IN2P3 et Université de la Méditerranée, 163 Avenue de Luminy, Case 902, 13288 Marseille Cedex 9, France
- <sup>c</sup>GRPHE - Institut universitaire de technologie de Colmar, 34 rue du Grillenbreit BP 50568 - 68008 Colmar, France
- <sup>d</sup>INFN - Sezione di Genova, Via Dodecaneso 33, 16146 Genova, Italy
- <sup>e</sup>Friedrich-Alexander-Universität Erlangen-Nürnberg, Erlangen Centre for Astroparticle Physics, Erwin-Rommel-Str. 1, D-91058 Erlangen, Germany
- <sup>f</sup>Direction des Sciences de la Matière - Institut de recherche sur les lois fondamentales de l'Univers - Service d'Electronique des Détecteurs et d'Informatique, CEA Saclay, 91191 Gif-sur-Yvette Cedex, France
- <sup>g</sup>Institut d'Investigació per a la Gestió Integrada de Zones Costaneres (IGIC) - Universitat Politècnica de València. C/ Paranimf, 1. E-46730 Gandia, Spain.
- <sup>h</sup>FOM Instituut voor Subatomaire Fysica Nikhef, Science Park 105, 1098 XG Amsterdam, The Netherlands
- <sup>i</sup>INFN - Sezione di Bari, Via E. Orabona 4, 70126 Bari, Italy
- <sup>j</sup>APC - Laboratoire AstroParticule et Cosmologie, UMR 7164 (CNRS, Université Paris 7 Diderot, CEA, Observatoire de Paris) 10, rue Alice Domon et Léonie Duquet 75205 Paris Cedex 13, France
- <sup>k</sup>LAM - Laboratoire d' Astrophysique de Marseille, Pôle de l' Étoile Site de Château-Gombert, rue Frédéric Joliot-Curie 38, 13388 Marseille cedex 13, France
- <sup>l</sup>Dipartimento di Fisica dell'Università, Viale Berti Pichat 6/2, 40127 Bologna, Italy
- <sup>m</sup>INFN - Sezione di Bologna, Viale Berti Pichat 6/2, 40127 Bologna, Italy
- <sup>n</sup>Dipartimento di Fisica dell'Università ?La Sapienza?, P.le Aldo Moro 2, 00185 Roma, Italy
- <sup>o</sup>INFN -Sezione di Roma, P.le Aldo Moro 2, 00185 Roma, Italy
- <sup>p</sup>Clermont Université, Université Blaise Pascal, CNRS/IN2P3, Laboratoire de Physique Corpusculaire, BP 10448, F-63000 Clermont-Ferrand, France
- <sup>q</sup>Dipartimento di Fisica dell'Università, Largo B. Pontecorvo 3, 56127 Pisa, Italy
- <sup>r</sup>INFN - Sezione di Pisa, Largo B. Pontecorvo 3, 56127 Pisa, Italy
- <sup>s</sup>INAF-IASF, via P. Gobetti 101, 40129 Bologna, Italy
- <sup>t</sup>Géozur - Université de Nice Sophia-Antipolis, CNRS/INSU, IRD, Observatoire de la Côte d'Azur and Université Pierre et Marie Curie ? F-06235, BP 48, Villefranche-sur-mer, France
- <sup>u</sup>INFN - Laboratori Nazionali del Sud (LNS), Via S. Sofia 62, 95123 Catania, Italy
- <sup>v</sup>Direction des Sciences de la Matière - Institut de recherche sur les lois fondamentales de l'Univers - Service de Physique des Particules, CEA Saclay, 91191 Gif-sur-Yvette Cedex, France
- <sup>w</sup>COM - Centre d'Océanologie de Marseille, CNRS/INSU et Université de la Méditerranée, 163 Avenue de Luminy, Case 901, 13288 Marseille Cedex 9, France
- <sup>x</sup>Université Paris-Sud 11 - Département de Physique - F - 91403 Orsay Cedex, France
- <sup>y</sup>IPHC-Institut Pluridisciplinaire Hubert Curien - Université de Strasbourg et CNRS/IN2P3 23 rue du Loess -BP 28- F67037 Strasbourg Cedex 2
- <sup>z</sup>Royal Netherlands Institute for Sea Research (NIOZ), Landsdiep 4,1797 SZ 't Horntje (Texel), The Netherlands
- <sup>aa</sup>Kernfysisch Versneller Instituut (KVI), University of Groningen, Zernikelaan 25, 9747 AA Groningen, The Netherlands
- <sup>ab</sup>Universiteit Utrecht, Faculteit Betawetenschappen, Princetonplein 5, 3584 CC Utrecht, The Netherlands
- <sup>ac</sup>Universiteit van Amsterdam, Instituut voor Hoge-Energie Fysika, Science Park 105, 1098 XG Amsterdam, The Netherlands
- <sup>ad</sup>Dipartimento di Fisica ed Astronomia dell'Università, Viale Andrea Doria 6, 95125 Catania, Italy
- <sup>ae</sup>University of Wisconsin - Madison, 53715, WI, USA
- <sup>af</sup>Institute for Space Sciences, R-77125 Bucharest, Măgurele, Romania
- <sup>ag</sup>Dipartimento di Fisica dell'Università, Via Dodecaneso 33, 16146 Genova, Italy

## Abstract

The AMADEUS system described in this article is integrated into the ANTARES neutrino telescope in the Mediterranean Sea and aims at the investigation of techniques for acoustic detection of neutrinos in the deep sea. Installed at water depths between 2000 and 2400 m, its acoustic sensors employ piezo-electric elements for the broad-band recording of signals with frequencies ranging up to 125 kHz with typical sensitivities around  $-145$  dB re.  $1\text{V}/\mu\text{Pa}$  (including preamplifier). Completed in May 2008, AMADEUS consists of six “acoustic clusters”, each comprising six acoustic sensors that are arranged at distances of roughly 1 m from each other. Three acoustic clusters each are installed along two vertical mechanical structures (so-called lines) of the ANTARES detector at a horizontal distance of 240 m. Vertical spacings within a line range from 15 m to 125 m. Each cluster contains custom-designed electronics boards to amplify and digitise the acoustic data from the sensors. The data transmission to shore is done via optical fibres, using the TCP/IP protocol. An on-shore computer cluster, currently consisting of four dedicated servers, is used to process, filter and store the selected data. The daily volume of recorded data is about 10 – 20 GByte. The system is operating continuously and automatically, requiring only little human intervention. AMADEUS allows for extensive studies of both transient signals and ambient noise in the deep sea as well as signal correlations on several length scales and localisation of acoustic point sources. Thus the system is excellently suited to assess the background conditions that affect the measurement of bipolar pulses expected to originate from neutrino interactions. This in turn allows for feasibility studies of a future large-scale acoustic neutrino telescope in the Mediterranean Sea.

*Key words:* AMADEUS, ANTARES, Neutrino telescope, Acoustic neutrino detection, Thermo-acoustic model

*PACS:* 95.55.Vj, 95.85.Ry, 13.15.+g, 43.30.+m

---

## 1 Introduction

2 The use of acoustic pressure pulses is a promising approach for the detection of  
3 cosmic neutrinos with energies exceeding 100 PeV in huge underwater acoustic ar-  
4 rays. The pressure signals are produced by the particle cascades that evolve when  
5 a neutrino interacts with a nucleus in the water. This energy deposition leads to a

---

\* Corresponding author

*Email address:* robert.lahmann@physik.uni-erlangen.de (R. Lahmann).

<sup>1</sup> Also at University of Leiden, the Netherlands

<sup>2</sup> On leave at DESY, Platanenallee 6, D-15738 Zeuthen, Germany

6 local heating of the medium which can be regarded as instantaneous with respect  
7 to the hydrodynamic time scale. According to the thermo-acoustic model [1,2], the  
8 medium expands or contracts according to its volume expansion coefficient as a re-  
9 sult of the temperature change. The accelerated motion of the heated volume forms  
10 a pressure pulse of bipolar shape in time—a micro-explosion—which propagates  
11 in the surrounding medium. The pulse has a characteristic frequency spectrum that  
12 is expected to peak around 10 kHz after propagating several hundreds of metres in  
13 sea water in the direction perpendicular to the shower axis [3,4]. Besides sea water,  
14 which is the medium under investigation in the case of the AMADEUS<sup>3</sup> project,  
15 ice [5] and fresh water [6] are investigated as media for acoustic detection of neu-  
16 trinos. Studies in sea water are also pursued by other groups using military arrays  
17 of underwater microphones (hydrophones) [7,8] or exploiting other existing deep  
18 sea infrastructures [9].

19 Two major advantages over an optical neutrino telescope make acoustic detection  
20 worth studying. First, the attenuation length in sea water is of the order of 5 km  
21 (1 km) for 10 kHz (20 kHz) signals. This is one to two orders of magnitude larger  
22 than for Cherenkov light in the relevant frequency band (attenuation length of the  
23 order of 60 m for blue light). Thus the sensor spacings in a potential future large-  
24 scale acoustic detector are not governed by the attenuation length but instead by  
25 the prerequisites set forth by the reconstruction requirements for neutrino events.  
26 The second advantage is the much simpler sensor design and readout electronics  
27 for acoustic measurements: No high voltage is required and for acoustic signals the  
28 time scales are in the  $\mu\text{s}$  range, where suitable off-the-shelf electronics is readily  
29 available, compared to the ns range for optical signals. This allows the online imple-  
30 mentation of advanced signal processing techniques. Efficient data filters are essen-  
31 tial, as the signal amplitude is relatively small compared to the acoustic background  
32 in the sea, which complicates the unambiguous determination of the signal. Since  
33 the sound velocity<sup>4</sup> is small compared to the speed of light, coincidence windows  
34 between two separated sensors are correspondingly large. For a high background  
35 rate, this can render the reconstruction of signals difficult to impossible if the sen-  
36 sor spacings are too large. To overcome this problem, while at the same time not  
37 sacrificing the advantages given by the large attenuation length, AMADEUS uses  
38 the concept of several spatially separated *local clusters*. This is described in Sec. 2.

39 The AMADEUS project was conceived to perform a feasibility study for a poten-  
40 tial future large scale acoustic detector. The project extends the ANTARES detec-  
41 tor [10,11] with a dedicated array of acoustic sensors. In the context of AMADEUS  
42 the following aims are being pursued:

- 43 • Long-term background investigations (rate of neutrino-like signals, spatial and

---

<sup>3</sup> ANTARES Modules for the Acoustic Detection Under the Sea.

<sup>4</sup> The speed of sound in sea water depends on temperature, salinity and pressure, i.e. depth. A good guideline value for the speed of sound at the location of AMADEUS is 1500 m/s.

- 44 temporal distributions of sources, levels of ambient noise);
- 45 ● Investigation of correlations for transient signals and for persistent background
  - 46 on different length scales;
  - 47 ● Development and tests of filter and reconstruction algorithms;
  - 48 ● Investigation of different types of acoustic sensors and sensing methods;
  - 49 ● Studies of hybrid (acoustic and optical) detection methods.

50 Especially the rate and correlation length of neutrino-like acoustic background  
51 events, in particular at the ANTARES site, is not known but is a prerequisite for  
52 estimating the sensitivity of such a detector.

53 In this paper, the AMADEUS system within the ANTARES detector is described.  
54 In Sec. 2, an overview of the system is given, with particular focus on its integra-  
55 tion into the ANTARES detector. In Sec. 3, the system components are described  
56 and in Sec. 4, the system performance discussed. The characteristic features of  
57 the AMADEUS system are mainly determined by two components: The acoustic  
58 sensors and the custom-designed electronics board, which performs the off-shore  
59 processing of the analogue data from the acoustic sensors. These two components  
60 are discussed in detail in Sections 3.1 and 3.4.

## 61 **2 Overview of the AMADEUS System**

### 62 *2.1 AMADEUS as part of the ANTARES detector*

63 AMADEUS is integrated into the ANTARES neutrino telescope [10] in the Mediter-  
64 ranean Sea, which was designed to reconstruct the tracks of up-going muons orig-  
65 inating from neutrino interactions by detecting the Cherenkov light induced by the  
66 passage of relativistic charged particles. The ANTARES detector was completed  
67 in May, 2008, by the installation of the last components. A sketch of the detector,  
68 with the AMADEUS modules highlighted, is shown in Fig. 1. The detector is lo-  
69 cated at a water depth of about 2500 m, about 40 km south of the town of Toulon on  
70 the French Mediterranean coast. It comprises 12 vertical structures, the *Detection*  
71 *Lines*, plus a 13th line, called *Instrumentation Line (IL)*, equipped with instruments  
72 for monitoring the environment. Each detection line holds 25 *storeys* that are ar-  
73 ranged at equal distances of 14.5 m along the line, starting at an altitude of about  
74 100 m above the sea bed and interlinked by electro-mechanical-optical cables. A  
75 standard storey consists of a titanium support structure, holding three *Optical Mod-*  
76 *ules* [12] (photomultiplier tubes (PMTs) inside water-tight pressure-resistant glass  
77 spheres) and one *Local Control Module (LCM)*. The LCM contains the off-shore  
78 electronics and a power supply within a cylindrical titanium container (cf. Sec. 3.3).  
79 The IL holds six storeys, all of which are non-standard. The vertical distance be-  
80 tween consecutive storeys is increased to 80 m for two pairs of storeys in the IL.



81 Each line is fixed on the sea floor by an anchor equipped with electronics and held  
 82 vertically by an immersed buoy. An interlink cable connects each line to the *Junc-*  
 83 *tion Box* from where the main electro-optical cable provides the connection to the  
 84 shore station.

85 The ANTARES lines are free to swing and rotate in the undersea currents. In order  
 86 to determine the positions of the storey with a precision of about 20 cm—as  
 87 required to achieve the specified pointing precision of reconstructed muon tracks—  
 88 the detector is equipped with an acoustic positioning system [13]. The system em-  
 89 ploys an acoustic transceiver at the anchor of each line and up to four autonomous  
 90 transponders positioned around the 13 lines. Along each detection line, five po-  
 91 sitioning hydrophones receive the signals of the emitters. By performing multiple  
 92 time delay measurements and using these to triangulate the individual hydrophones,  
 93 the line shapes can be reconstructed relative to the positions of the emitters. Cur-  
 94 rently, the sequence of signal emissions required for the positioning is emitted every  
 95 2 minutes.

96 In AMADEUS, acoustic sensing is integrated in form of *Acoustic Storeys* which are  
 97 modified versions of standard ANTARES storeys, replacing the OMs by custom-  
 98 designed acoustic sensors and using dedicated electronics for the digitisation and  
 99 preprocessing of the analogue signals.

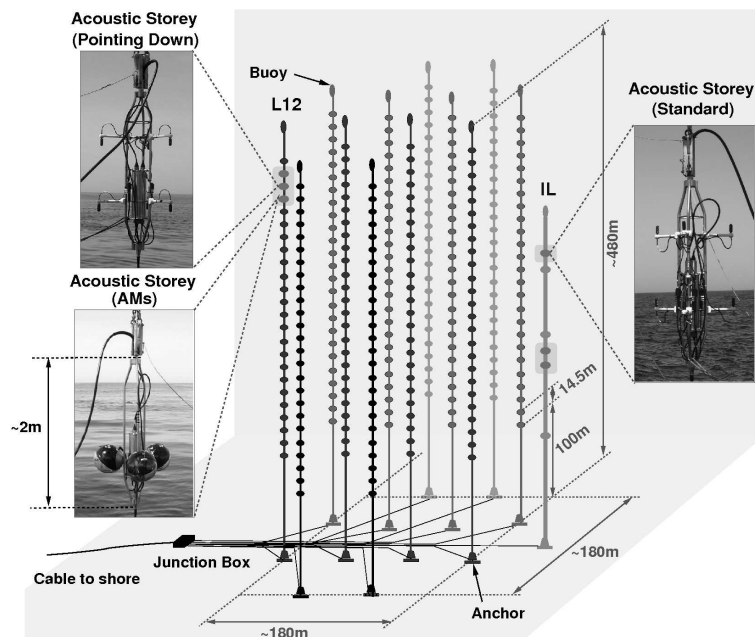


Figure 1. A sketch of the ANTARES detector. The six Acoustic Storeys are highlighted and their three different setups are shown. L12 and IL denote Line 12 and the Instrumentation Line, respectively.

100 The AMADEUS system comprises a total of six Acoustic Storeys: Three on the  
 101 IL, which started data taking when the connection to shore of the IL was made  
 102 in December 2007; and three on Line 12 which were connected to shore during

103 the completion of the ANTARES detector in May 2008. AMADEUS is now fully  
104 functional and routinely taking data with 34 sensors<sup>5</sup>.

105 The Acoustic Storeys on the IL are located at 180 m, 195 m, and 305 m above the  
106 sea floor. On Line 12, which is anchored at a horizontal distance of about 240 m  
107 from the IL, the Acoustic Storeys are positioned at heights of 380 m, 395 m, and  
108 410 m above the sea floor. With this setup, the maximum distance between two  
109 Acoustic Storeys is 340 m. AMADEUS hence covers three length scales: spacings  
110 of the order of 1 m between sensors within a storey forming a cluster; intermediate  
111 distances of about 15 m between adjacent Acoustic Storeys within a line; and large  
112 scales from about 100 m vertical distance on the IL up to 340 m between storeys on  
113 different lines. The sensors within a cluster allow for triggering and for direction  
114 reconstruction; the directional reconstruction from different Acoustic Storeys can  
115 then be combined for the position reconstruction of acoustic sources [14]. The sys-  
116 tem has full detection capabilities—including time synchronisation and a continu-  
117 ously operating system for long-term data acquisition—and is scalable to a larger  
118 number of Acoustic Storeys.

## 119 2.2 Acoustic Storeys

120 Two types of sensing devices are used in AMADEUS: hydrophones and *Acoustic*  
121 *Modules* (AMs). The sensors are in both cases based on the piezo-electric effect  
122 and are discussed in Sec. 3.1. Figure 2 shows the design of a standard Acoustic  
123 Storey with hydrophones.

124 The three Acoustic Storeys on the IL house hydrophones only, whereas the lower-  
125 most Acoustic Storey of Line 12 holds AMs (cf. Fig. 3(a)). In the central Acoustic  
126 Storey of Line 12, the hydrophones were exceptionally mounted to point down-  
127 wards (cf. Fig. 3(b)), largely reducing the upwardly sensitivity. This allows for in-  
128 vestigating the directionality of background from ambient noise, which is expected  
129 to come mainly from the sea surface.

130 Three of the five storeys holding hydrophones are equipped with commercial mod-  
131 els, dubbed “HTI hydrophones<sup>6</sup>”, and the other two with hydrophones developed  
132 and produced at the Erlangen Centre for Astroparticle Physics (ECAP), described  
133 in detail in Sec. 3.1.

---

<sup>5</sup> Two out of 36 hydrophones became inoperational during the initial deployment. No further deterioration of the performance has been observed since then.

<sup>6</sup> Custom produced by High Tech Inc (HTI) in Gulfport, MS (USA).

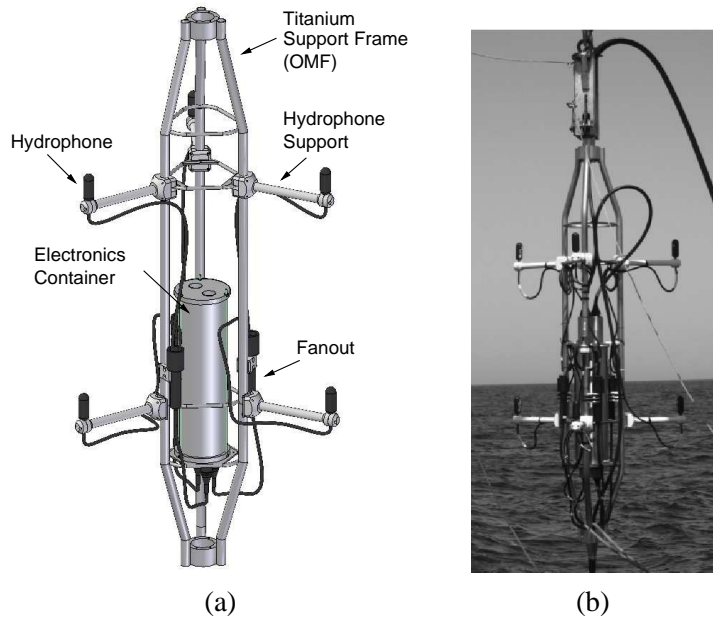


Figure 2. (a) Drawing of a standard Acoustic Storey with hydrophones; (b) photograph of a standard storey during deployment (central Acoustic Storey on the Instrumentation Line).

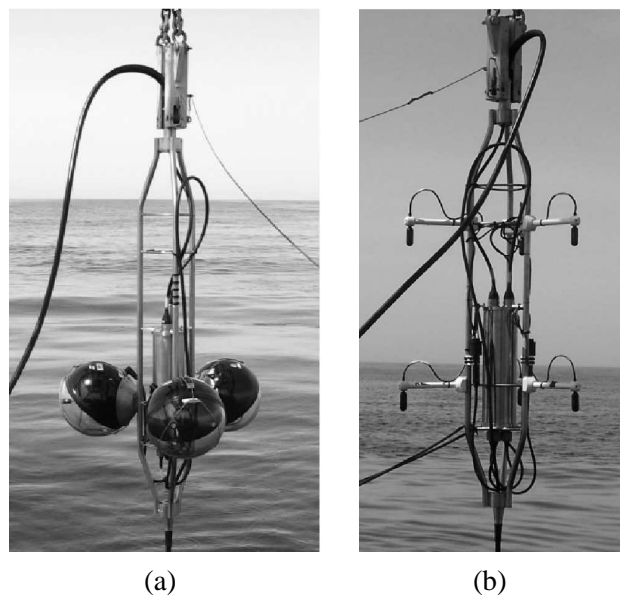


Figure 3. Photographs of the two non-standard storeys of the AMADEUS system during their deployment: (a) The lower-most Acoustic Storey on Line 12 equipped with Acoustic Modules; (b) the central Acoustic Storey on Line 12 with the hydrophones pointing down.

134 **2.3 Design Principles**

135 A fundamental design guideline for the AMADEUS system has been to use existing  
 136 ANTARES hard- and software as much as possible. In this way the design efforts

137 were kept to a minimum and new quality assurance and control measures had to be  
138 introduced only for the additional components, which were subjected to an inten-  
139 sive testing procedure. The high water pressure of up to 250 bar and the salinity of  
140 the water constitute a hostile environment that imposes strong requirements on the  
141 material of the detector.

142 In order to integrate the AMADEUS system into the ANTARES detector, design  
143 and development efforts in the following basic areas were necessary:

- 144 ● The development of acoustic sensing devices that replace the Optical Modules  
145 of standard ANTARES storeys and of the cables to route the signals into the  
146 electronics container;
- 147 ● The development of an off-shore acoustic digitisation and preprocessing board;
- 148 ● The setup of an on-shore server cluster for the online processing of the acoustic  
149 data and the development of the online software;
- 150 ● The development of offline reconstruction and simulation software.

151 Six acoustic sensors per storey were implemented. This number was the maximum  
152 compatible with the design of the LCM and the bandwidth of data transmission to  
153 shore. Furthermore, the length of the hydrophone supports (cf. Fig. 2) was chosen  
154 to not exceed the diameter of the spheres of the Optical Modules, hence assuring  
155 compatibility with the deployment procedure of the ANTARES lines.

#### 156 2.4 *The AMADEUS-0 Test Apparatus*

157 In March 2005, a full-scale mechanical prototype line for the ANTARES detector  
158 was deployed and subsequently recovered [15] for leak-testing the titanium LCM  
159 containers and investigating the behaviour of the inter-storey electro-optical cable  
160 and its connectors under pressure. This line, dubbed *Line 0*, contained no photomul-  
161 tipliers and no readout electronics. Instead, a miniature autonomous data logging  
162 system and shore-based optical time-domain reflectometry were used to record the  
163 status of the setup.

164 Line 0 provided a well-suited environment to study the properties of the acoustic  
165 sensors in-situ at a time when the readout electronics for AMADEUS was still in  
166 the planning phase and the piezo-preamplifier setup in the design phase. For this  
167 purpose, an autonomous system within a standard LCM container, the AMADEUS-  
168 0 device, was integrated into Line 0. It recorded acoustic noise at the ANTARES  
169 site using five piezo sensors with custom-designed preamplifiers, glued to the inside  
170 of the LCM container. A battery-powered readout and data logging system was  
171 devised and implemented using commercially available components. The system  
172 was further equipped with a timing mechanism to record data over two pre-defined  
173 periods: The first one lasted for about 10 hours and included the deployment of  
174 the line. During this period, a total of 2:45 hours of data were taken over several

175 intervals. In the second period, with the line installed on the sea floor, 1:45 hours of  
176 data were taken over a period of 3:30 hours until the battery power was exhausted.

177 The analysis of the data [16] provided valuable information for the design of the  
178 AMADEUS system. In particular, the level of the recorded noise allowed for tuning  
179 the sensitivity and frequency response of the preamplifiers and amplifiers of the  
180 AMADEUS system.

### 181 **3 System Components**

#### 182 *3.1 The Acoustic Sensors*

183 The fundamental components of both the hydrophones and the Acoustic Modules  
184 are piezo-electrical ceramics, converting pressure waves into voltage signals [17],  
185 and preamplifiers. A schematic view of an ECAP hydrophone is shown in Fig. 4.  
186 For these hydrophones <sup>7</sup> two-stage preamplifiers were used: Adapted to the capaci-  
187 tive nature of the piezo elements and the low induced voltages, the first preamplifier  
188 stage is charge integrating while the second one is amplifying the output voltage of  
189 the first stage. The shape of the ceramics is that of a hollow cylinder.

190 Due to hardware constraints of the electronics container, the only voltage available  
191 for the operation of the hydrophone preamplifiers was 6.0 V. In order to minimise  
192 electronic noise, the hydrophone preamplifiers was designed for that voltage rather  
193 than employing DC/DC converters to obtain the 12.0 V supply more typically used.

194 The piezo elements and preamplifiers of the hydrophones are coated in polymer  
195 plastics. Plastic endcaps prevent the material from pouring into the hollow part of  
196 the piezo cylinder during the moulding procedure. All hydrophones have a diameter  
197 of 38 mm and a length (from the cable junction to the opposite end) of 102 mm.  
198 The hydrophones produced at ECAP were designed to match the dimensions of the  
199 sensors ordered from HTI.

200 The equivalent inherent noise level in the frequency range from 1 to 50 kHz is about  
201 13 mPa for the ECAP hydrophones and about 5.4 mPa for the HTI hydrophones.  
202 This compares to 6.2 mPa of the lowest expected ambient noise level in the same  
203 frequency band for a completely calm sea [18].

204 At the ANTARES site, the hydrophones are subject to an external pressure of 200 –  
205 240 bar. Prior to deployment, each hydrophone was pressure-tested in accordance

---

<sup>7</sup> For the commercial hydrophones, details were not disclosed by the manufacturer, but the main design is similar to the one described here.

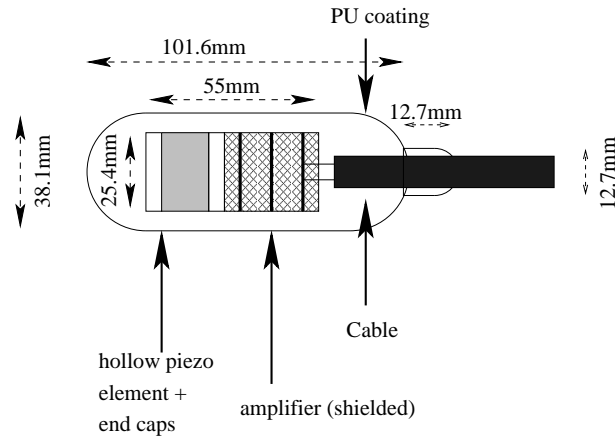


Figure 4. Schematic view of an ECAP hydrophone. Piezo and preamplifier are moulded into polyurethane (PU).

206 with ANTARES rules, i.e. the pressure was ramped up to 310 bar at 12 bar per  
 207 minute, held there for two hours and then ramped down again at 12 bar per minute.

208 For the AMs, the same preamplifiers are used as for the ECAP hydrophones. The  
 209 piezo elements have the same outer dimensions but in the shape of a solid cylinder.  
 210 Two sensors are glued to the inside of each of the spheres normally used for the  
 211 Optical Modules of the ANTARES detector. This design was inspired by the idea  
 212 to investigate an option for acoustic sensing that can be combined with a PMT  
 213 in the same housing. In order to assure an optimal acoustic coupling, the space  
 214 between the curved sphere and the flat end of the piezo sensor of the AM was filled  
 215 with epoxy. A photograph of an Acoustic Module and a schematic drawing of the  
 216 sensors glued to the inside of the glass sphere are shown in Fig. 5.

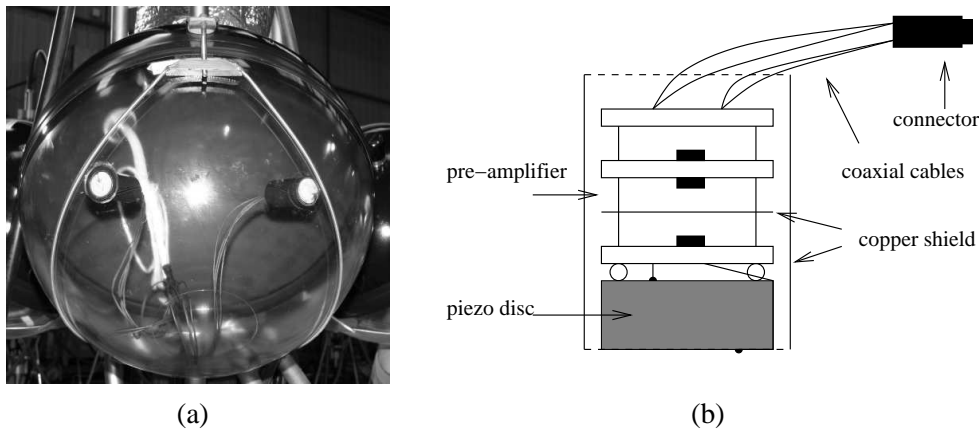


Figure 5. (a) Photograph of an Acoustic Module (AM) before deployment; (b) schematic drawing of an AM sensor.

217 In order to obtain a complete  $2\pi$ -coverage of the azimuthal angle  $\phi$ , the 6 sensors  
 218 are distributed over the three AMs of the storey within the plane defined by the  
 219 three nominal centres of the spheres. The two sensors in each sphere are separated  
 220 by an angle of  $60^\circ$  with respect to the centre of the sphere. The sphere has an outer

221 diameter of 432 mm at atmospheric pressure.

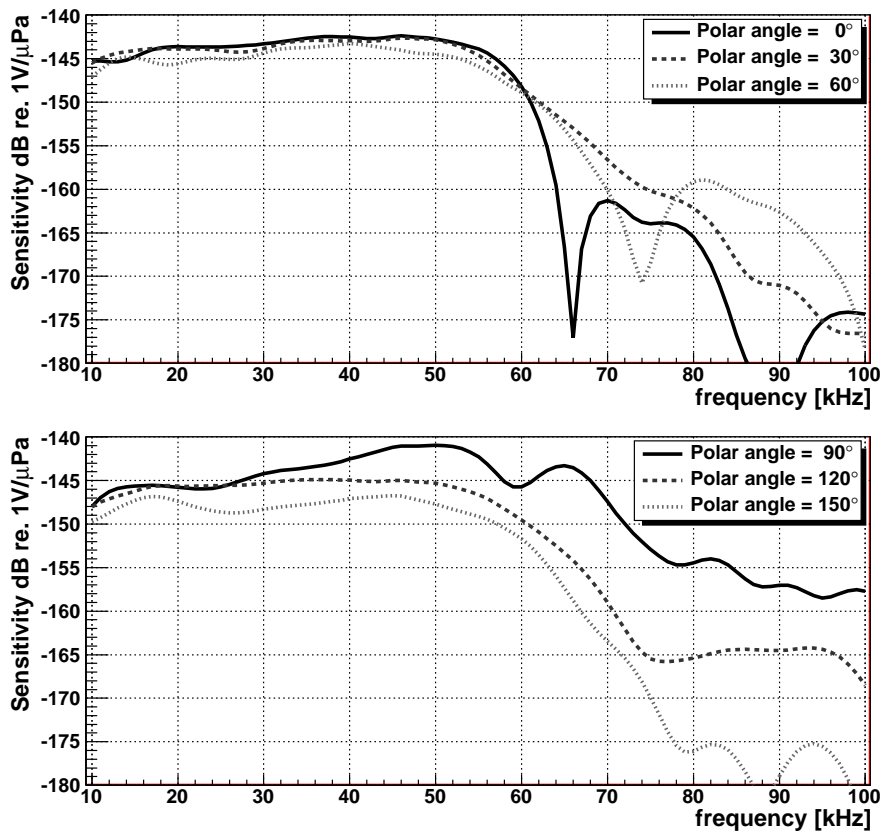


Figure 6. Typical sensitivity of an HTI hydrophone as a function of frequency for different polar angles.

222 All sensors are tuned to have a low noise level and to be sensitive over the frequency  
223 range from 1 to 50 kHz with a typical sensitivity around  $-145$  dB re.  $1\text{V}/\mu\text{Pa}$  (in-  
224 cluding preamplifier). The sensitivity of one of the commercial hydrophones is  
225 shown in Fig. 6 as a function of frequency for different polar angles [19]. For fre-  
226 quencies below 50 kHz, the sensitivity decreases once the polar angle approaches  
227  $180^\circ$ , which defines the direction at which the cable is attached to the hydrophone.  
228 The beginning of this trend can be seen for the polar angle of  $150^\circ$ .

229 The sensitivity as a function of the azimuthal angle for a given frequency is es-  
230 sentially flat at the 3 dB level. The sensitivity as a function of solid angle and fre-  
231 quency shows no significant deviations between different HTI hydrophones in the  
232 frequency range from 10 to 50 kHz. The variations for the hydrophones produced  
233 at ECAP are larger, at a level of 3 – 4 dB.

234 3.2 *Cables*

235 Each acoustic sensor requires a total of four leads for individual power supply and  
236 differential signal readout. In order to connect two hydrophones to one of the three  
237 connectors in the electronics container, special *fanout cables* were produced (cf.  
238 Fig. 2). For the connection to the SubConn<sup>8</sup> connector sockets of the electronics  
239 container, the same mating connector plugs as for the OMs—with redefined pin  
240 assignments—were used.

241 At the other end of the cable, a bulkhead connector AWQ-4/24 of the ALL-WET  
242 split series by Seacon<sup>9</sup> was moulded. Each bulkhead connector fans out into six  
243 wedge-shaped sectors, into two of which the mating 4-pin connectors, moulded to  
244 a neoprene cable with the hydrophone, are inserted. The remaining four sectors  
245 of the bulkhead connector are sealed with blind plugs. All 15 fanout cables used  
246 within AMADEUS are functioning as expected.

247 The standard cables used in the ANTARES detector between the electronics con-  
248 tainer and the OMs are also used to connect the AMs to the LCM with the pinning  
249 redefined to match that for the hydrophones. The LCMs integrated into storeys with  
250 AMs and with hydrophones are equivalent.

251 3.3 *Off-Shore Electronics*

252 In the ANTARES data acquisition (DAQ) scheme [20], the digitisation is done  
253 within the off-shore electronics container (cf. Sec. 2). Each LCM contains a back-  
254 plane that is equipped with the connectors for the electronics cards and provides  
255 power and data lines to and from the connectors. A standard LCM for processing  
256 the data from PMTs contains the following electronics boards:

- 257 ● Three *ARS motherboards* comprising two Analogue Ring Sampler (ARS) ASICs  
258 each for conditioning and digitisation of the analogue data from the PMTs [21];
- 259 ● A *DAQ board*, which reads out the ARS motherboards and handles the commu-  
260 nication to the shore via TCP/IP;
- 261 ● A *Clock board* that provides the timing signals to correlate measurements per-  
262 formed in different storeys (cf. Sec. 3.6).
- 263 ● A *Compass board* that measures the tilt and the orientation of the storey.

264 The transmission of data to shore is done through Master LCMs (MLCMs) which—  
265 in addition to the components of an LCM described above—contain an Ethernet

---

<sup>8</sup> MacArtney Underwater Technology group, <http://www.subconn.com>.

<sup>9</sup> Seacon (Europe) LTD, Great Yarmouth, Norfolk, UK. Seacon also manufactured the fanout cables.



266 Switch and additional boards for handling incoming and outgoing fibre-based op-  
267 tical data transmission. Up to five storeys form a sector, for which the individual  
268 LCMs transmit the data to the MLCM.

269 For the digitisation of the acoustic signals and for feeding them into the ANTARES  
270 data stream, the *AcouADC board* was designed. They are pin-compatible with the  
271 ARS motherboards and replace those in the Acoustic Storeys. Figure 7 shows the  
272 fully equipped LCM of an Acoustic Storey.

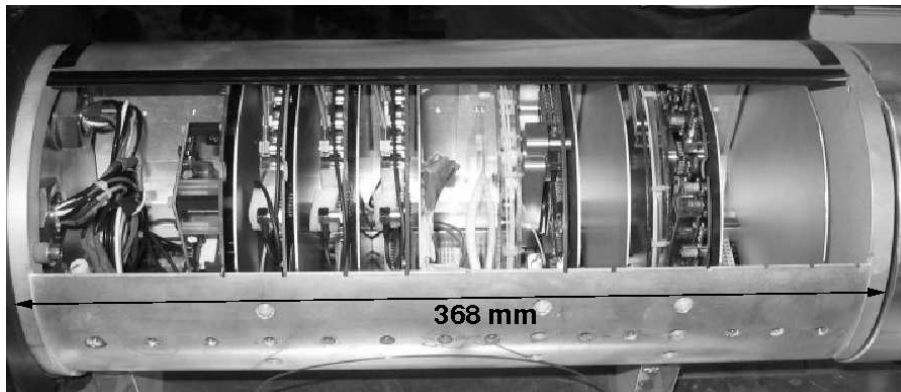


Figure 7. An LCM equipped with AcouADC boards before insertion into its titanium housing. From left to right, the following boards are installed: a Compass board; three AcouADC boards; a DAQ board; a Clock board.

### 273 3.4 The AcouADC Board

274 The AcouADC board has the following major tasks:

- 275 ● Preprocessing of the analogue data for the digitisation (impedance matching,  
276 application of an anti-alias filter, selectable gain adjustment) for two acoustic  
277 sensors;
- 278 ● Digitisation of the analogue data and preparation of the digitised data stream for  
279 the serial transmission to the DAQ-board;
- 280 ● Provision of two stable low-noise voltage lines (6V) for the power supply of two  
281 hydrophones;
- 282 ● Provision of an interface to the on-shore control software to set the run parame-  
283 ters (cf. Sec. 3.5).

284 A photograph and a block diagram of an AcouADC board are shown in Figs. 8 and  
285 9, respectively. The board consists of an analogue and a digital part. Each board  
286 processes the differential voltage signals from two acoustic sensors, referred to as  
287 “Sig 0” and “Sig 1” in the diagram. The two signals are processed independently  
288 and in parallel for the complete (analogue and digital) data processing chain.

289 A main design criterion for the board was low noise, such that even for a completely  
290 calm sea no significant contribution to the recorded noise signal originates from the  
291 electronics of the board. To protect the analogue parts from potential electromag-  
292 netic interference, they are shielded by metal covers. Tests of the electromagnetic  
293 compatibility (EMC) of the board have shown that this design is vulnerable to elec-  
294 tromagnetic noise only for conditions that are far more unfavourable than those  
295 expected in situ; and even then only at a level that does not significantly affect the  
296 acoustic measurements [18].

297 The two 6V power supply lines on each AcouADC board (connectors labeled “Pow  
298 0” and “Pow 1” in Fig. 9) are protected by resettable fuses against short circuits that  
299 could be produced by the sensors due to water ingress. In addition, each voltage  
300 line can be individually switched on or off.

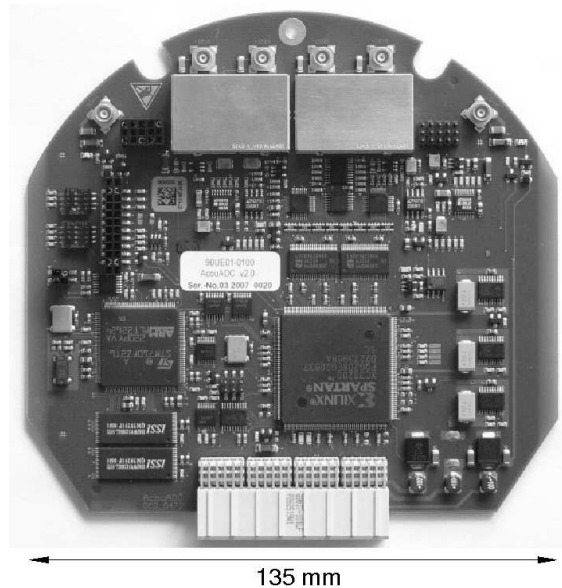


Figure 8. An AcouADC board. The four connectors for the two differential input signals are located at the top, the analogue signal processing electronics is covered by metal shields. The two 6V power connectors are located to the left and right of the shields.

### 301 3.4.1 Analogue Part

302 In the analogue part each signal is amplified in two stages. The first stage applies  
303 a coarse gain with nominal amplification factors of 1, 10 or 100. It is implemented  
304 as a differential amplifier with single-ended output, referenced to 2.5 V. The gain  
305 factor 1 is used to record dedicated runs of signals with a large amplitude (e.g. from  
306 the emitters of the ANTARES acoustic positioning system (cf. Sec. 2.1)), whereas  
307 the factor of 100 is a safety feature in case the sensitivity of the hydrophones should  
308 drop significantly due to the long-term exposure to the high pressure.

309 The second amplification stage, the fine gain, is intended to adjust the gains of  
310 different types of hydrophones. It is a non-inverting amplification with single ended

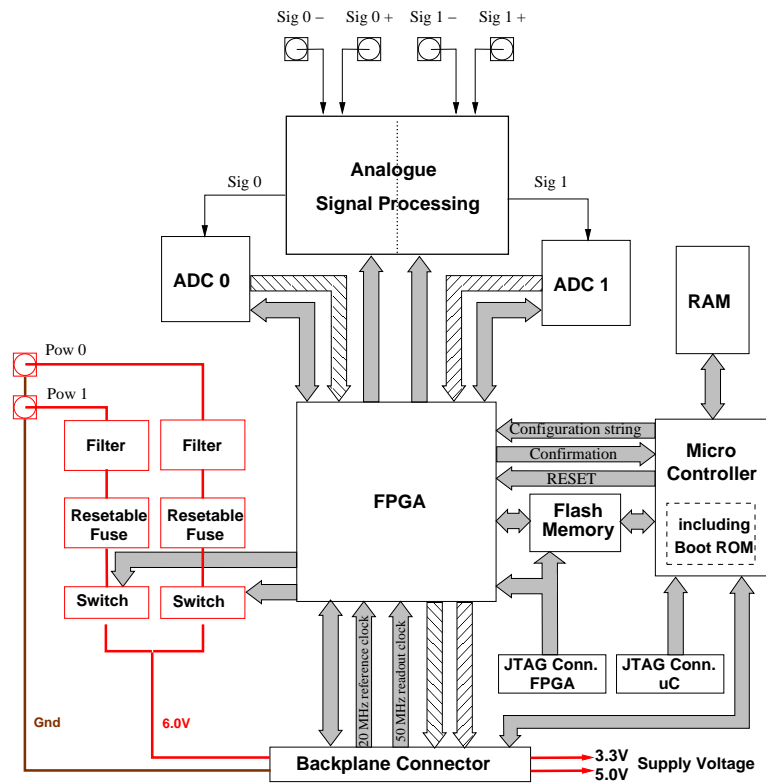


Figure 9. Block diagram of the AcouADC board. The flow of the analogue sensor signals is indicated by thin arrows, hatched arrows denote the flow of the digitised data further downstream. General communication connections are shown as shaded arrows; some signals are denoted by their names. The components relevant for the power supply of the hydrophones are shown in the left part. Voltage supply lines are indicated by thick lines. Connectors are indicated as squares with inlaying circles.

311 output and a reference voltage of 2.5 V. Gain factors of 1.00, 1.78, 3.16, and 5.62  
 312 (corresponding to 0, 5, 10, and 15 dB, respectively) are selectable by switching  
 313 between four appropriate resistors in the feedback loop of the operational amplifier.  
 314 Combining the two stages, the gain can be set to one of 12 factors between 1 and  
 315 562. The standard setting is an overall gain factor of 10.

316 After amplification in the two stages described above, the signal is coupled into a  
 317 linear-phase 10th-order anti-alias filter with a root-raised cosine amplitude response  
 318 and a 3 dB point at  $f_{\text{cutoff}} = 128 \text{ kHz}$ <sup>10</sup>. In low-power mode, the filter output has  
 319 a typical maximal point-to-point amplitude of 3.9 V. The output is referenced to  
 320 2.0 V and fed into the analogue-to-digital converter (ADC). Accordingly, the ADC  
 321 reference voltage is set to 2.0 V, implying that the digital output of zero corresponds  
 322 to this analogue value, with an input range from 0.0 to 4.0 V.

323 The three analogue stages (coarse and fine amplification and anti-alias filtering)  
 324 and the ADC are decoupled by appropriate capacitors. Furthermore, several RCL

<sup>10</sup> Filter LTC1569-7 from Linear Technology.

325 elements within the analogue signal chain form an additional band pass filter: A  
326 high-pass filter with a 3dB point of about 4kHz cuts into the trailing edge of the  
327 low-frequency noise of the deep-sea acoustic background [22] and thus protects  
328 the system from saturation. Additional RCL elements forming passive filters were  
329 implemented to comply with the input requirements of active components of the  
330 circuitry.

### 331 3.4.2 Digital Part

332 The digital part of the AcouADC board digitises and processes the acoustic data.  
333 It is highly flexible due to the use of a micro controller ( $\mu\text{C}$ )<sup>11</sup> and a field pro-  
334 grammable gate array (FPGA)<sup>12</sup> as data processor. The  $\mu\text{C}$  can be controlled with  
335 the on-shore control software and is used to adjust settings of the analogue part and  
336 the data processing. Furthermore, the  $\mu\text{C}$  can be used to update the firmware of the  
337 FPGA in situ. All communication with the shore is done by the  $\mu\text{C}$  via the DAQ  
338 board. For laboratory operation, JTAG connectors to access the FPGA,  $\mu\text{C}$ , and the  
339 flash memory are provided. The latter stores the firmware loaded into the FPGA  
340 when it is reset. In-situ, the reset is asserted from the  $\mu\text{C}$ . If a firmware update is  
341 performed, the  $\mu\text{C}$  first loads the code from the shore into the random access mem-  
342 ory (RAM). Only when the integrity of the code has been confirmed by means of  
343 a checksum, the code is transmitted into the flash memory. In order to avoid the  
344 potential risk that a software error renders the  $\mu\text{C}$  inaccessible, its boot ROM can  
345 only be changed in the laboratory.

346 The digitisation is done at 500 kSps (kSamples per second) by one 16-bit ADC<sup>13</sup>  
347 for each of the two input channels. The digitised data from the two channels is read  
348 out in parallel by the FPGA and further formatted for transmission to the DAQ  
349 board.

350 ADCs do commonly show relatively high deviations from a linear behaviour near  
351 the zero point of their digital range. The size of this effect depends on the circuitry  
352 into which the ADC is embedded. For the prototypes of the AcouADC boards, this  
353 effect proved to be fairly pronounced. For this reason, the reference voltage of the  
354 anti-alias filter output can be switched from its standard value of 2.0 V to 1.0 V,  
355 thereby moving the peak of the noise distribution away from the digital value of  
356 zero.

357 In standard mode, the sampling rate is reduced to 250 kSps in the FPGA, corre-  
358 sponding to a downsampling by a factor of 2 (DS2). Hence the frequency spectrum  
359 of interest from 1 to 100 kHz is fully contained in the data. Currently implemented  
360 is a choice between DS1 (i.e. no downsampling), DS2, and DS4, which can be set

<sup>11</sup> STR710 from STMicroelectronics.

<sup>12</sup> Spartan-3 XC3S200 from Xilinx.

<sup>13</sup> ADS8323 successive approximation ADC from Analog Devices.

361 from the shore. Each downsampling factor requires an adapted digital anti-alias fil-  
 362 ter that is implemented in the FPGA as finite impulse response (FIR) filter with a  
 363 length of 128 data points.

### 364 3.4.3 System Characteristics

365 The complex response function of the AcouADC board (i.e. amplitude and phase)  
 366 was measured in the laboratory prior to deployment for each board and a physically  
 367 motivated parameterisation of the function was derived [18]. Fig. 10 shows the fre-  
 368 quency response of the AcouADC board. The measurement was done by feeding  
 369 Gaussian white noise into the system and analysing the digital output recorded by  
 370 the board. Without downsampling (DS1), the rolloff at high frequencies is gov-  
 371 erned by the analogue anti-alias filter. For DS2 and DS4, the digital FIR filters are  
 372 responsible for the behaviour at high frequencies. At low frequencies, the effect of  
 373 the high-pass filter described above can be seen. Fig. 10 shows furthermore that  
 374 within each passband, the filter response is essentially flat. The comparison of the  
 375 recorded data with the parameterisation shows excellent agreement.

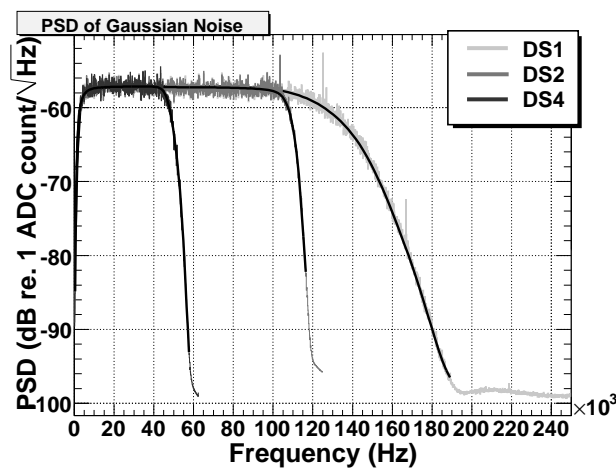


Figure 10. The filter response, characterised as power spectral density (PSD) as a function of the frequency, measured for the three different downsampling factors. For each of the three measurements, the parameterisation is shown as a black line.

376 Fig. 11 shows a comparison of the measured and calculated response to a bipolar  
 377 input pulse as it would be expected from a neutrino shower (cf. Sec. 1). The digital  
 378 FIR filter would introduce an additional time offset of  $128 \mu\text{s}$  of the digitised data  
 379 for downsampling factors 2 and 4.

380 The ADCs of the AcouADC board were investigated in detail [18]. For each indi-  
 381 vidual ADC, the transfer curve from input voltage to least significant bits (LSBs)<sup>14</sup>

<sup>14</sup> The LSB is commonly used to denote one ADC count; the full-scale digital range for a 16-bit ADC is therefore 65535 LSB.

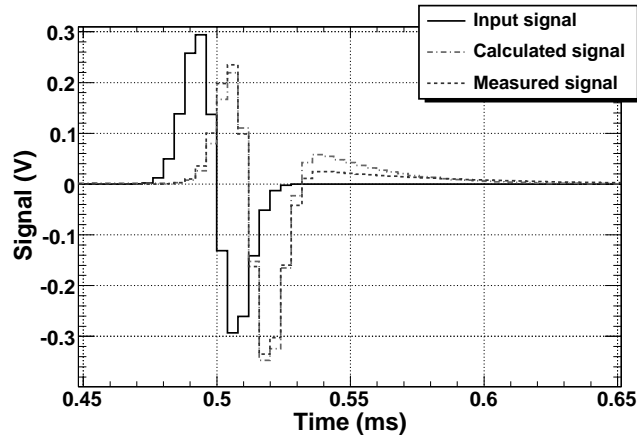


Figure 11. The response of an AcouADC board to a bipolar input pulse. Shown are the measured signal and the signal calculated from the parameterised response function. The measured signal was obtained with an oscilloscope at the input of the ADC. The measurement was done for a nominal gain factor of 1.

382 was measured and distortions from the ideal linear behaviour quantified in terms of  
 383 the differential nonlinearity (DNL) and integral nonlinearity (INL).

384 The spurious-free dynamic range (SFDR) of an ADC is defined as the strength  
 385 ratio of the fundamental signal to the strongest spurious signal in the output and  
 386 is a measure of the dynamic range of the ADC. Using a sinusoidal input signal,  
 387 the average SFDR of the ADCs of all boards in AMADEUS was measured to be  
 388  $(59.9 \pm 1.1)$  dB, meaning that harmonics of the sine wave distorting the signal are  
 389 suppressed by 3 orders of magnitude in the amplitude. Hence a clear determina-  
 390 tion of the frequency even for saturated signals—for which typically the harmonic  
 391 components are enhanced—is possible.

392 Each individual gain factor for each channel was calibrated and the correction factor  
 393 for gain 1 was measured to be  $0.95 \pm 0.01$ . Deviations with respect to this value for  
 394 the 11 other settings were found to be largest with a level of about 10% for the  
 395 coarse gain of 100 with no significant dependence on the fine gain factor.

396 The inherent noise of the electronics (output for open signal input) and the cross  
 397 talk (output for open signal 0 or 1, when the other input is fed with a signal) were  
 398 confirmed to be negligible in comparison with the characteristics of the acoustic  
 399 sensors.

### 400 3.5 Slow Control System

401 The ANTARES Slow Control (SC) system has two main tasks: It provides the off-  
 402 shore components with initialisation and configuration parameters and it regularly  
 403 monitors whether the operational parameters are within the specified range. In ad-

404 dition, the readout of some instruments for environmental monitoring [23] (which  
405 is done at intervals of a few minutes) is polled and sent through the SC interface.

406 For the AMADEUS system, the following parameters can be set from the shore via  
407 the SC system for each acoustic channel individually: one of 12 values for the gain;  
408 downsampling factor of 1, 2, or 4 (or no data transmission from the AcouADC  
409 board); the power supply for the acoustic sensor can be switched on or off; and the  
410 reference voltage of the analogue signal fed into the ADC can be switched between  
411 2.0 V and 1.0 V.

412 To monitor the environment within each LCM container, a humidity sensor and  
413 temperature sensors on several boards are installed. One temperature sensor is  
414 placed on each AcouADC board. Values read out by the SC system are stored in  
415 one Oracle® database, hosted at the IN2P3<sup>15</sup> computing centre at Lyon, that is  
416 centrally used for all needs of ANTARES and AMADEUS.

### 417 3.6 *Data Acquisition and Clock System*

418 AMADEUS follows the same “all data to shore” strategy [20] as the ANTARES  
419 neutrino telescope, i.e. all digitised data are transmitted to shore via optical fibres,  
420 using the TCP/IP protocol. The data stream from the sender DAQ board is tagged  
421 with the IP address of the receiving on-shore server. In the ANTARES control room,  
422 the data arrive at a Gigabit switch in exactly the same fashion as the data from the  
423 PMTs. At the switch the acoustic data are separated from the optical data and routed  
424 to the acoustic server cluster based on the transmitted IP address.

425 The ANTARES clock system operates separately from the DAQ system, using a  
426 different set of optical fibres to synchronise data from different storeys. The system  
427 provides a highly stable 20 MHz synchronisation signal, corresponding to a resolu-  
428 tion of 50 ns<sup>16</sup>, which is generated by a custom-designed system at the ANTARES  
429 control room. The synchronisation of this internal clock with the UTC time of the  
430 GPS system is established with a precision of 100 ns.

431 The synchronisation signal is broadcasted to the off-shore clock boards and from  
432 there transmitted further to the FPGA of the AcouADC board. Based on this sig-  
433 nal, the data packages sent from the AcouADC board to shore via the DAQ board  
434 receive a time stamp which allows an offline correlation of the data from different  
435 storeys. The 50 ns resolution of the time stamp corresponds to a resolution of less  
436 than 0.1 mm of a sound wave travelling at 1500 m/s in water which far exceeds the

---

<sup>15</sup> Institut National de Physique Nucléaire et de Physique des Particules (France).

<sup>16</sup> The much higher precision that is required for the synchronisation of the optical signals from the PMTs is provided by a 256-fold subdivision of the 20 MHz signal in the ARS motherboards.

437 required precision. Differences in the signal transit times between the shore station  
438 and the individual storeys are of the order of  $1\ \mu\text{s}$  and are small enough that they  
439 do not need to be corrected for.

### 440 3.7 On-Shore Data Processing and Run Control

441 The AMADEUS system is operated with a dedicated run control software that was  
442 adapted from the standard ANTARES software called *RunControl* [20]. The latter  
443 is a program with a graphical user interface to control and operate the experiment.  
444 It is Java-based and reads the configuration of the individual hard- and software  
445 components from the ANTARES database, allowing for an easy adaption to the  
446 AMADEUS system. Via the database, the RunControl allows for defining differ-  
447 ent detector setups which may vary in the specified run parameters or may have  
448 individual storeys removed in case of hardware problems. Via the clock system the  
449 absolute time of the run start is logged in the database with the aforementioned  
450 precision of 100 ns. Events recorded during the run then have a timing precision  
451 of 50 ns with respect to the start of the run. The end of a run is reached if either a  
452 predefined size or duration of the recorded data has been reached (in which case a  
453 new run is started automatically) or the run is stopped by the operator. The data of  
454 one AMADEUS run are stored in a single file in root format [24], the typical length  
455 of a run is 2 to 5 hours.

456 Even though the DAQ system was not designed to operate multiple RunControl  
457 programs in parallel, the system proved flexible enough to handle this situation  
458 without interference between the runs of AMADEUS and of the ANTARES neu-  
459 trino telescope.

460 For the computing requirements of AMADEUS, a dedicated on-shore computer  
461 cluster was installed. It currently consists of four servers, of which two are used for  
462 data triggering<sup>17</sup> (2 HP ProLiant DL380 G5 with  $2\times$  dual core 3 GHz Intel Xeon  
463 5160 and  $2\times$  quad core 3 GHz Intel Xeon 5450 processors, respectively). Hence, a  
464 total of 12 cores are available to process the data received from the ANTARES GBit  
465 switch. One of the remaining two servers is used to write the data to an internal 550  
466 GByte disk, while the other server is used to operate the RunControl software and  
467 miscellaneous other processes. The latter server also provides remote access to the  
468 system via the Internet.

469 The AMADEUS trigger searches the data by an adjustable software filter; the  
470 events thus selected are stored to disk. This way the raw data rate of about 1.5 TB/day  
471 is reduced to about 15 GB/day for storage. Currently, three trigger schemes are in  
472 operation [25]: A minimum bias trigger which records  $\sim 10$  s of continuous data

---

<sup>17</sup> While this functionality might be more commonly referred to as filter system, it is ANTARES convention to refer to the “on-shore trigger”.



473 every 60 min; a threshold trigger which is activated when the signal exceeds a pre-  
474 defined amplitude; and a pulse shape recognition trigger. For the latter, a cross  
475 correlation of the signal with a predefined bipolar signal, as it is expected to be  
476 recorded for a neutrino shower, is performed. The trigger condition is met if the  
477 output of the cross correlation operation exceeds a predefined threshold. This trig-  
478 ger corresponds to a matched filter for a white noise background.

479 Both, the threshold and the pulse shape recognition trigger are applied to the indi-  
480 vidual sensors and are self-adjusting to the ambient noise, implying that all trigger  
481 thresholds are defined in terms of a signal to noise ratio. The trigger thresholds are  
482 freely adjustable. If one of these two trigger conditions is met, an additional trig-  
483 ger condition is imposed, which requires coincidences of a predefined number of  
484 acoustic sensors on each storey. The coincidence window is fixed to the length of  
485 about 105 ms of a *frame*, i.e. the structure in which data are buffered off-shore by  
486 the DAQ-board before being sent to shore [20]. Currently, the coincidence trigger  
487 requires that the threshold or pulse shape recognition trigger conditions have been  
488 met for at least four out of six sensors.

489 For reasons stemming from the fact that the ANTARES DAQ system was designed  
490 to comply with the nanosecond time scales of an optical neutrino telescope, the  
491 coincidence window is not implemented as a sliding window but starts at fixed  
492 intervals with respect to the run start. However, given the distances of typically 1 m  
493 between sensors within one storey, time delays between signals from a given source  
494 are always less than 1 ms. Therefore the number of sources for which the signals  
495 extend over two frames, and hence the coincidence trigger may not be activated, is  
496 small. The coincidence trigger can be optionally extended to require coincidences  
497 between different storeys on the same line. With distances between storeys ranging  
498 from about 10 m to 100 m (and delays therefore reaching the order of 10 ms to  
499 100 ms) the coincidence window in this case suppresses signals originating from  
500 above or below. This trigger level is currently not enabled.

501 Once the coincidence trigger has fired, the data within a time window are stored.  
502 First, a window of 2.56 ms (corresponding to 640 data samples at 4 $\mu$ s sampling  
503 time) is defined around the point in time when the trigger condition was met. Then  
504 adjacent or overlapping windows are merged. Consequently, data are stored for  
505 each sensor within time windows with a length ranging from 2.56 ms to  $\sim$ 105 ms.

506 The triggers of the AMADEUS system and the main ANTARES optical neutrino  
507 telescope are working completely independently. Hence the search for potentially  
508 correlated signals does rely on offline analyses.

509 All components of the AMADEUS system are scalable which makes it very flex-  
510 ible. Additional servers can be added or the existing ones can be replaced by new  
511 generation models if more sophisticated trigger algorithms are to be implemented.  
512 In principle it is also possible to move parts of the trigger algorithm into the FPGA

513 of the AcouADC board, thereby implementing an off-shore trigger which reduces  
514 the size of the data stream sent to shore.

515 Just like the ANTARES neutrino telescope, AMADEUS can be controlled via the  
516 Internet and is currently operated from ECAP. Data are centrally stored and are  
517 available remotely as well.

## 518 **4 System Performance**

519 AMADEUS is continuously operating and taking data with only a few interventions  
520 by the RunControl operator per week. The on-time of each sensor is about 75 to  
521 80% and is defined as the ratio between the time over which the sensor is taking  
522 data and the active time of that sensor. Not active were only those times during  
523 which the power or data transmission to shore was interrupted due to problems that  
524 required a sea operation for maintenance.

525 The concept of local clusters (i.e. the storeys) is very efficient for fast online pro-  
526 cessing. By requiring coincident signals from at least four sensors within a storey,  
527 the rate of the cross correlation trigger is reduced by a factor of more than 20 with  
528 respect to the rate of a single sensor when using the same thresholds.

529 The parallel operation of two separate RunControl programs for AMADEUS and  
530 the main ANTARES neutrino telescope has proven to be very successful. No in-  
531 terference between the two programs has been observed while the two systems  
532 can optimise their detection efficiency and respond to potential problems almost  
533 independently. At the same time, both systems profit in the same fashion from de-  
534 velopments and improvements of the RunControl.

535 The stability of the system is excellent. This was verified prior to deployment as  
536 well as in-situ. It was quantified by observing the mean of the ambient noise distri-  
537 bution as a function of time. In-situ, the 10 s of continuous data recorded every hour  
538 with the minimum bias trigger were used for the measurement. The worst observed  
539 RMS variation of this value for the first year of operation is less than  $2 \cdot 10^{-5}$  of  
540 the full range (65535 LSB or 4.0 V).

541 Studies of the power spectral density of the ambient noise at the ANTARES site  
542 have been performed using the minimum bias trigger data. The lowest level of  
543 recorded noise in situ was confirmed to be consistent with the intrinsic noise of the  
544 system recorded in the laboratory prior to deployment (cf. Fig. 12). The observed  
545 in-situ noise can be seen to go below the noise level measured in the laboratory  
546 for frequencies exceeding 35 kHz. This is due to electronic noise coupling into the  
547 system in the laboratory that is absent in the deep sea. Above that same frequency,  
548 the intrinsic electronic noise starts to dominate over the mean ambient noise. This

549 frequency consequently constitutes an upper bound for studies of the ambient noise  
550 in the deep sea with AMADEUS.

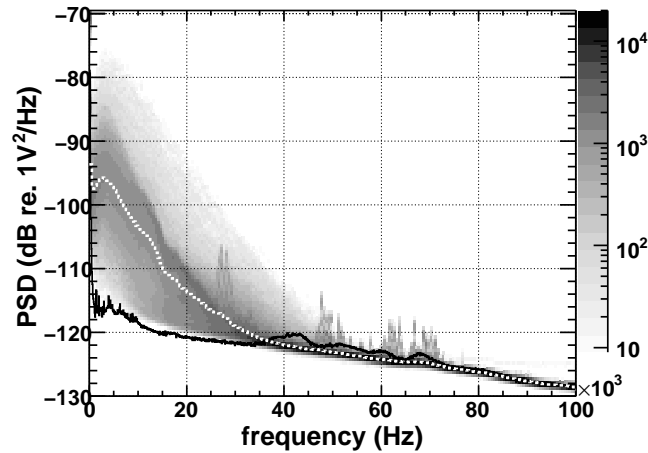


Figure 12. Power spectral density (PSD) of the ambient noise recorded with one sensor on the topmost storey of the IL. Shown in shades of grey is the occurrence rate in arbitrary units, where dark colours indicate higher occurrence rates. Shown as a white dotted line is the mean value of the in-situ PSD and as a black solid line the noise level recorded in the laboratory prior to deployment.

551 Using the same minimum bias data, a further demonstration can be done that the  
552 recorded data are indeed representative of the ambient conditions and not deter-  
553 mined by the intrinsic noise of the system: the noise levels (i.e. the RMS of the  
554 signal amplitudes in each 10 s sample) recorded at the same time with any two ac-  
555 tive sensors are highly correlated with correlation coefficients between 93% and  
556 100%.

557 The AMADEUS cross correlation trigger selects signals for which the signal to  
558 noise ratio exceeds a value of about 2 for a bipolar signal recorded with a single  
559 acoustic sensor. Assuming a noise level of 10 mPa for the frequency range of 1  
560 to 100 kHz, which represents the scale for a combination of the equivalent intrin-  
561 sic sensor noise and the lowest ambient noise for a calm sea, the corresponding  
562 recorded pressure signal would be emitted from a 2 EeV cascade for a neutrino in-  
563 teraction at a distance of 200 m [3]. Using a cross correlation trigger with a signal  
564 shape more closely adjusted to the expected signal from a neutrino shower, the en-  
565 ergy threshold can be further reduced. This threshold, determined by the ambient  
566 noise, is the optimal achievable energy threshold for the detection of neutrinos. The  
567 rate at which neutrino-like signals are mimicking neutrino interactions will then set  
568 a more stringent limit. This rate is subject to investigation and will be a decisive in-  
569 dication concerning the feasibility of a future large scale acoustic neutrino detector.

570 The maximal pressure amplitude that can be recorded for a gain factor of 10 without  
571 saturating the input range of the ADC is about 5 Pa. Usually only anthropogenic  
572 signals originating close to the detector reach this pressure level.

573 The position reconstruction of acoustic point sources is currently being pursued as  
574 one of the major prerequisite to identify neutrino-like signals. Simulation results  
575 are presented in [14].

576 Just as for the standard storeys holding PMTs, the relative positions of the Acoustic  
577 Storeys within the detector have to be continuously monitored. This is done by us-  
578 ing the emitter signals of the ANTARES acoustic positioning system (cf. Sec. 2.1).  
579 Fig. 13 shows such a signal as recorded by four representative sensors. The delays  
580 between the signal arrivals are clearly visible: short delays of less than 1 ms within  
581 each storey and a long delay of about 10 ms between the signals arriving in two  
582 different storeys.

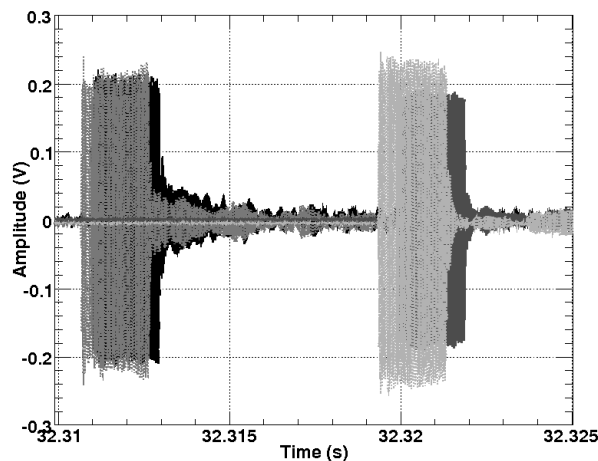


Figure 13. Typical emitter signals of the ANTARES acoustic positioning system as recorded with four sensors of the AMADEUS system. The first two signals along the time axis were recorded by the Acoustic Storey holding AMs (cf. Fig. 1). The following two signals were recorded with two hydrophones on the Acoustic Storey just above—one hydrophone mounted at the bottom and the other one at the top of a storey. All signals were recorded with a gain factor 1 of the AcouADC board. The time is counted since the start of the run.

583 The time shown in the Figure is given in seconds since the start of the run and can be  
584 converted into UTC time using the data recorded by the clock system (cf. Sec. 3.6).  
585 As the emission times of the positioning signals are also recorded in UTC time,  
586 the time difference between emission and reception of the signal can be calculated.  
587 Using the signals from multiple emitters and their known positions at the anchors  
588 of the lines, the positions of the AMADEUS sensors can be reconstructed.

589 The positioning accuracy for each hydrophone shows statistical errors of a few  
590 mm for the hydrophones. The final measurement is expected to be dominated by  
591 systematic uncertainties due to the physical size of the receiving piezo elements, the  
592 knowledge of their relative positions within the acoustic storey, and the knowledge  
593 of the speed of sound in sea water. For the AMs, the position reconstruction is less  
594 precise and statistical and systematic uncertainties are expected to be of the same

595 order of magnitude.

596 As a recent development, marine scientists have become interested in the data  
597 recorded by AMADEUS for the study of marine mammals, in particular cetaceans.  
598 The system hence will be used as a multipurpose apparatus for neutrino feasibility  
599 studies, acoustic positioning and marine research.

## 600 **5 Summary and Conclusions**

601 The AMADEUS system for the investigation of techniques for acoustic particle de-  
602 tection in the deep sea has been integrated into the ANTARES neutrino telescope  
603 in the Mediterranean Sea at water depths between 2000 and 2400 m. The system  
604 started taking data in December 2007 and was completed in May 2008. The system  
605 consists of 36 acoustic sensors, of which currently 34 are operational, arranged in  
606 six acoustic clusters. Different sensor setups and different installations of the acous-  
607 tic clusters are in operation. The sensors are based on piezo-electric elements and  
608 two-stage preamplifiers with combined sensitivities around  $-145$  dB re.  $1\text{V}/\mu\text{Pa}$ .

609 Data sampling is done at 500 kSps with 16 bits and an analogue anti-alias filter  
610 with a 3 dB point at  $f_{\text{cutoff}} = 128$  kHz. One of twelve steps of analog amplification  
611 between 1 to 562 can be set with the on-shore control software. Digital downsam-  
612 pling with factors of 2 and 4 is implemented inside an off-shore FPGA. The value  
613 is also selectable using on-shore control software.

614 All components of the system have been calibrated in the laboratory prior to de-  
615 ployment; the in-situ performance is in full accordance with the expectations. Data  
616 taking is going on continuously and the data are recorded if one of three adjustable  
617 trigger conditions is met.

618 The system is well suited to conclude on the feasibility of a future large scale  
619 acoustic neutrino telescope in the deep sea. Furthermore, it has the potential of  
620 a multi-purpose device, combining its design goal to investigate acoustic neutrino  
621 detection techniques with the potential to perform marine science and the ability  
622 for positioning. AMADEUS hence is a promising starting point for instrumenting  
623 the future neutrino telescope project KM3NeT [26,27] with acoustic sensors for  
624 calibration and science purposes.

## 625 **6 Acknowledgments**

626 The authors acknowledge the financial support of the funding agencies: Centre Na-  
627 tional de la Recherche Scientifique (CNRS), Commissariat à l’Energie Atomique

628 (CEA), Commission Européenne (FEDER fund and Marie Curie Program), Région  
629 Alsace (contrat CPER), Région Provence-Alpes-Côte d'Azur, Département du Var  
630 and Ville de La Seyne-sur-Mer, in France; Bundesministerium für Bildung und  
631 Forschung (BMBF), grants 05A08WE1, 05A08WEA, and 05CN5WE1/7 in Ger-  
632 many; Istituto Nazionale di Fisica Nucleare (INFN), in Italy; Stichting voor Fun-  
633 damenteel Onderzoek der Materie (FOM), Nederlandse organisatie voor Weten-  
634 schappelijk Onderzoek (NWO), in the Netherlands; Russian Foundation for Basic  
635 Research (RFBR), in Russia; National Authority for Scientific Research (ANCS)  
636 in Romania; Ministerio de Ciencia e Innovación (MICINN), in Spain. We also ac-  
637 knowledge the technical support of Ifremer, AIM and Foselev Marine for the sea  
638 operation and the CC-IN2P3 for the computing facilities.

## 639 References

- 640 [1] G.A. Askariyan, B.A. Dolgoshein et al., *Acoustic Detection of High Energy Particle*  
641 *Showers in Water*, NIM **164** (1979) 267
- 642 [2] J.G. Learned, *Acoustic Radiation by Charged Atomic Particles in Liquids: An*  
643 *Analysis*, PR **19** (1979) 3293
- 644 [3] S. Bevan et al. (ACoRNE Coll.), *Simulation of Ultra High Energy Neutrino*  
645 *Interactions in Ice and Water*, Astropart. Phys. **28** (2007) 366, arXiv:astro-  
646 ph/0704.1025v1
- 647 [4] S. Danaher et al. (ACoRNE Coll.), *Study of the Acoustic Signature of UHE Neutrino*  
648 *Interactions in Water and Ice*, arXiv:0903.0949v2 [astro-ph.IM] (2009)
- 649 [5] F. Descamps for the IceCube Coll., *Acoustic detection of high energy neutrinos in ice:*  
650 *Status and results from the South Pole Acoustic Test Setup*, in *Proceedings of the 31st*  
651 *International Cosmic Ray Conference*, (2009), arXiv:0908.3251v2 [astro-ph.IM]
- 652 [6] K. Antipin et al.(BAIKAL Coll.), *A prototype device for acoustic neutrino detection in*  
653 *Lake Baikal*, in *Proceedings of the 30th International Cosmic Ray Conference*, (2007),  
654 arXiv:0710.3113 [astro-ph]
- 655 [7] J. Vandenbroucke, G. Gratta and N. Lehtinen, *Experimental Study of Acoustic*  
656 *Ultra-high-Energy Neutrino Detection*, Astrophys. J. **621** (2005) 301, arXiv:astro-  
657 ph/0406105
- 658 [8] S. Danaher for the ACoRNE Coll., *First Data from ACoRNE and Signal Processing*  
659 *Techniques*, in *Proceedings of ARENA 2006 - Acoustic and Radio EeV Neutrino*  
660 *detection Activities*, J. Phys. Conf. Ser. **81** (2007) 012011
- 661 [9] NEMO Coll., *NEMO-O $\nu$ DE: a submarine station for real-time monitoring of acoustic*  
662 *background installed at 2000 m depth in the Mediterranean Sea*, submitted to Deep  
663 Sea Research I, arXiv:0804.2913v1 [astro-ph] (2008)
- 664 [10] The ANTARES Collaboration, *The ANTARES Neutrino Telescope in the*  
665 *Mediterranean Sea*, to be submitted to NIM A

- 666 [11] M. Ageron et al. (ANTARES Coll.), *Performance of the First ANTARES Detector*  
667 *Line*, *Astropart. Phys.* **31** (2009) 277, arXiv: 0812.2095 v1 [astro-ph]
- 668 [12] P. Amram et al. (ANTARES Coll.), *The ANTARES optical module*, *NIM A* **484** (2002)  
669 369
- 670 [13] M. Ardid for the ANTARES Coll., *Positioning system of the ANTARES neutrino*  
671 *telescope*, *NIM A* **602** (2009) 174
- 672 [14] C. Richardt et al., *Reconstruction methods for acoustic particle detection in the deep*  
673 *sea using clusters of hydrophones*, *Astropart. Phys.* **31** (2009) 19, arXiv:0906.1718v1  
674 [astro-ph.IM]
- 675 [15] M. Ageron et al. (ANTARES Coll.), *Studies of a full-scale mechanical prototype line*  
676 *for the ANTARES neutrino telescope and tests of a prototype instrument for deep-sea*  
677 *acoustic measurements*, *NIM A* **581** (2007) 695
- 678 [16] F. Deffner,  
679 *Studie zur akustischen Neutrinodetektion: Analyse und Filterung akustischer Daten*  
680 *aus der Tiefsee*, Diploma Thesis, Univ. Erlangen-Nürnberg, (2007, FAU-PI1-DIPL-  
681 07-001, obtainable from <http://www.antes.physik.uni-erlangen.de/publications>)
- 682 [17] G. Anton et al. *Study of piezo based sensors for acoustic particle detection*, *Astropart.*  
683 *Phys.* **26** (2006) 301
- 684 [18] K. Graf, *Experimental Studies*  
685 *within ANTARES towards Acoustic Detection of Ultra-High Energy Neutrinos in the*  
686 *Deep Sea*, Doctoral Thesis, Univ. Erlangen-Nürnberg, (2008, FAU-PI1-DISS-08-001,  
687 obtainable from <http://www.antes.physik.uni-erlangen.de/publications>)
- 688 [19] C.L. Naumann, *Development of Sensors for the Acoustic Detection of Ultra High*  
689 *Energy Neutrinos in the Deep Sea*,  
690 Doctoral Thesis, Univ. Erlangen-Nürnberg, (2007, FAU-PI4-DISS-07-002, obtainable  
691 from <http://www.antes.physik.uni-erlangen.de/publications>)
- 692 [20] J.A. Aguilar et al. (ANTARES Coll.), *The data acquisition system for the ANTARES*  
693 *neutrino telescope*, *NIM A* **570** (2007) 107
- 694 [21] The ANTARES Collaboration, *Performances of the front-end electronics of the*  
695 *ANTARES neutrino telescope*, to be submitted to *NIM A*
- 696 [22] R.J. Urick, *Principles of Underwater Sound* (Peninsula publishing, Los Altos, USA,  
697 1983)
- 698 [23] J.A. Aguilar et al. (ANTARES Coll.), *First results of the Instrumentation Line for the*  
699 *deep-sea ANTARES neutrino telescope*, *Astropart. Phys.* **26** (2006) 314
- 700 [24] The root homepage, <http://root.cern.ch/>
- 701 [25] M. Neff, *Studie zur akustischen Teilchendetektion im Rahmen des ANTARES-*  
702 *Experiments: Entwicklung und Integration von Datennahmesoftware*, Diploma  
703 Thesis, Univ. Erlangen-Nürnberg, (2007, FAU-PI1-DIPL-07-003, obtainable from  
704 <http://www.antes.physik.uni-erlangen.de/publications>)

- 705 [26] U.F. Katz et al. (KM3NeT Consortium), *Status of the KM3NeT project*, NIM A **602**  
706 (2009) 40
- 707 [27] KM3NeT Consortium, *Conceptual Design for a Deep-Sea Research Infrastructure*  
708 *Incorporating a Very Large Volume Neutrino Telescope in the Mediterranean Sea*,  
709 ISBN 978-90-6488-031-5, 2008, <http://www.km3net.org/CDR/CDR-KM3NeT.pdf>